# ON THE EXPERIMENTAL MEASUREMENT AND FEM SIMULATION OF THE DEFORMATION OF ROTATING CYLINDRICAL SHELLS DUE TO CENTRIFUGAL FORCES

**Marco A. Brujas, marco.brujas@voith.com**
Voith Paper Máquinas e Equipamentos Ltda

**Reyolando M.L.R.F. Brasil, reyolando.brasil@poli.usp.br**
Escola Politécnica da Universidade de São Paulo - PEF

*Abstract. Circular cylindrical shells, used in the paper industry, with small thickness variations along their body, when submitted to rotation, present, in some cases, elastic displacements of their outside surface induced by centrifugal forces leading to final oval like shapes. The main purpose of this study is to establish relationships between a given thickness variation of cylindrical shells with their measured deformation during the rotation, and results of finite element method (FEM) models. The studied cylindrical shells had their wall thickness measured by means of an ultrasound device. The used material is flake graphite cast iron (gray cast iron). The graphite flakes act as reflectors, what makes such measurements imprecise. The numerical results found are satisfactory in a qualitative way, but they disagree in the quantitative form. Shell models with theoretical imperfections also were created and analyzed using the finite element method in order to evaluate the behavior of the cylindrical shell under several configurations of distribution of the shell thickness variation. Further research is necessary on new technologies to measure the thickness of parts manufactured of flake graphite cast iron. The oval shape measurements were done by means of eddy-current proximity sensors.*

*Keywords: cylindrical shells, thickness variation, finite elements method, ultrasound, flake graphite cast iron.*

## 1. INTRODUCTION

The imperfections related to the manufacturing process of a part of equipment are characteristics inherent in any mechanical component. In particular in the paper manufacturing industry cylindrical equipment for web guidance during and after its formation are widely used, among which those of largest dimensions are called dryer cylinders (see Fig. 1), responsible for a part of water removal from the web by means of heat transmission during paper manufacturing machine operation. With the progress of manufacturing and operating techniques of such equipment in this type of industry, more and more the paper production speeds were increased, making the rotary equipment more sensitive to imperfections remaining from the manufacturing process. Thus, some equipment of this kind began recently to present excessive deformations on its cylindrical surface, of larger magnitude than similar equipment and increasing as rotational speed increased, suggesting the influence of centrifugal forces.

In an attempt to better evaluate the variations found and their causes, measurements of the dynamic form the cylindrical surface took during rotation were made at thirty-six cylinders of a same project. In addition, measurements of the thickness variation of its cylindrical shell were made by means of ultrasonic equipment all along the surface of the equipment.

The results indicated that dynamically the equipment took an oval shape, which developed as the rotational speed of the cylinder increased, resuming its original shape as rotation stopped, which characterized an elastic deformation. The thickness measurements showed a non-uniform mass distribution along the cylindrical shell, presenting in most cases an elliptical and eccentric distribution.

The purpose of this work is to establish the relationship between the cylindrical surface thickness variation and the oval shape arising due to the increase in rotational speed, by making critical use of numerical and experimental methods.
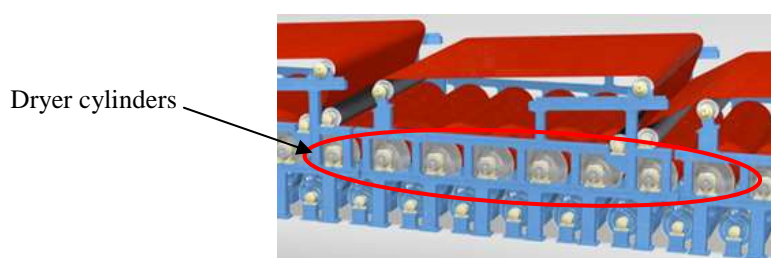


Figure 1 – Paper machine segment

## 2. METHODOLOGY

### 2.1. Obtention of experimental data

#### 2.1.1. Description of the physical models measured

The equipment on which the measurements were made basically consists of three parts: the cylindrical shell itself, heads for cylindrical shell support, and journals to support the whole assembly – see Fig. 2.
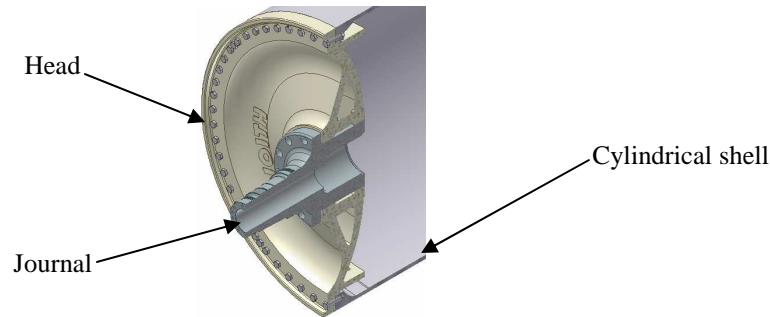
Head

Journal

Cylindrical shell

Figure 2 – Main parts of the model analyzed

#### 2.1.2. Model manufacturing process

The cylindrical shells are manufactured by casting, Pires (2006), in a vertical pit, by gravity, by using a sand core. The material employed in this case was SA 278 Class 40 (gray cast iron, or flake/lamellar graphite cast iron).

After dimensional controls and removal of segments from the ends - for manufacturing specimens for evaluating the mechanical and metallurgical properties -, the cylinder is machined both on the inside and outside on a horizontal lathe.

It is important to point out that the thickness variation distribution over this equipment does not occur symmetrically on the cylindrical shell centerline, but on its inside diameter.

The main dimensions of the analyzed shells were as follows: Length: *10070 mm,* Outside diameter: *1812 mm* ,Nominal thickness: *29 mm,* Mass: *≈18 t*

#### 2.1.3. Cylindrical shell ovalization measurement

To carry out the cylindrical shell ovalization measurements, inductive analog "eddy-current" (IA8-30GM-I3 model/ Pepperl) type motion sensors, horizontally arranged on either cylindrical shell side, have been used, as shown in Fig. 3. Measurements were made on a balancing unit, where rotation of which was carried out by means of a gear motor system coupled to the cylinder journal by a cardan shaft. The journals were simply supported on rollers, so as to allow axial motion of the equipment at the end opposite to the cardan shaft.

Based on these measurements, readings were processed by means of Fourier transforms, to obtain a polar diagram showing the dynamic cylinder shape (Fig. 4), as well as the signal decomposition into harmonics. Such measurements were made at constant rotational speed of 11.72 Hz.

Deflection from mean value

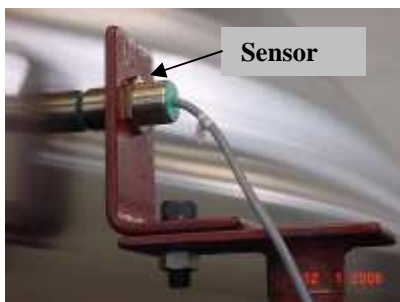**Sensor**

max-min = 836 μm

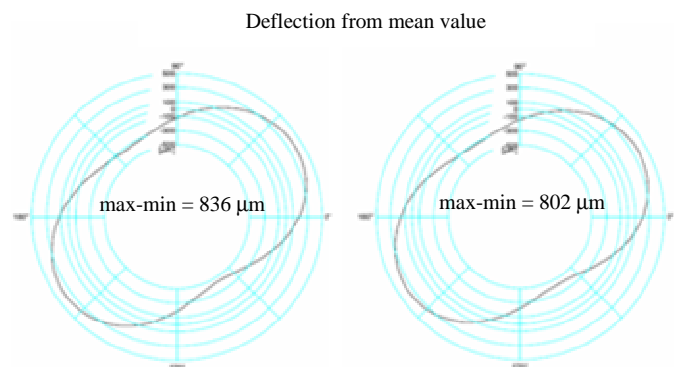max-min = 802 μm

Figure 3 – Sensor

Figure 4 – Dynamic shape according to the readings of the central sensors: front and rear

The reason for having sensors on either side of the cylindrical shell on the balancing machine is to be able to determine the external interference level or noise, that is being obtained at sensor readings. Logically, the front and rear sensor readings should result in identical values, only displaced by 180 degrees, but a small difference between them was always present, so that the results considered herein are mean values of both sensors readings.

In addition, the balancing machine has a laser displacement sensor (Fig. 5), which is positioned in the central bottom part of the equipment, with which the signals obtained are processed to obtain the harmonics composing of the motion of the cylindrical shell. These results are also presented in the form of graphs (Fig. 6), where the cylindrical shell harmonics amplitude evolution is observed as the speed increases.
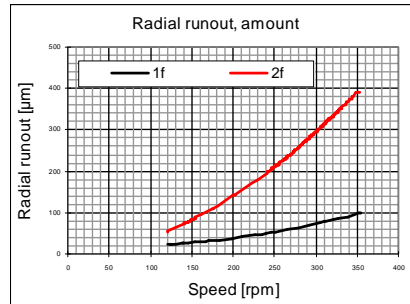


Figure 5 – Laser sensor



Figure 6 – Amplitude of harmonics

As well the ovalization measuring results obtained with the aid of inductive current sensors, as those obtained by the balancing machine, were taken sequentially to each other, immediately after balancing the equipment.

### 2.1.4. Comparison of measuring results

A good correlation between 2X results is observed in Fig. 8, except for five cylinders shown at the graph right–hand end (cylinders 6, 10, 12, 19, and 22), but in contrast to it Fig. 7, showing 1X results, presents a higher dispersion between the results, indicating only a correlation tendency between the points.
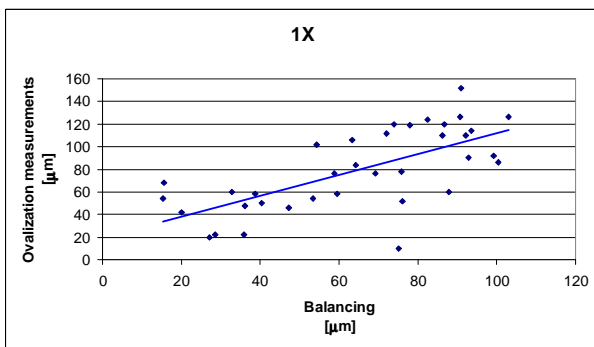


Figure 7 – Comparison of 1X of relationship
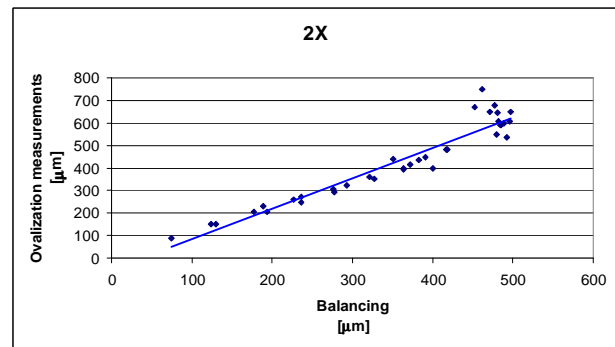between balancing machine results and measurements



Figure 8 – Comparison of 2X of relationship
between balancing machine results and measurements

A probable reason for this difference may be related to the magnitude of the results of both harmonics, the 2X results having a range of 74-570 μm, while the 1X ones just of 10-152 μm, which perhaps may indicate that for a same measuring error the values of lower magnitude would be more subject to deviations.

In general, the balancing machine sensor results are lower than those of the ovalization measurement. Possible causes might be: Inductive current sensors are not suitable for such measurements, sensor calibration, cable length and sensor support vibration.

### 2.1.5. Cylindrical shell thickness measurements

After assembly and final machining the cylindrical shells had their thicknesses measured by means of an ultrasonic apparatus (DM4 model collector and DA0.8 head, both manufactured by Krautkramer), so as to obtain a grid of the cylinder planned with the thickness variation mapping on its whole surface. The cylindrical shell was subdivided into 20 planes along its longitudinal axis, on each plane the outside circumference was subdivided into 28 equal segments

and the thickness of the position located at each subdivision crossing point was measured, totaling 560 points. Fig. 9 illustrates the surface division.
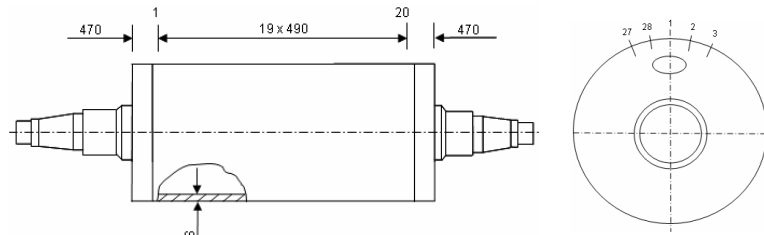


Figure 9 – Thickness measuring point schema

One knows according to TAPPI (2001) about the inaccuracy of carrying out thickness measurements in gray cast iron by ultrasound due to its metallurgical structure, considering the existence of graphite lamellae (Fig. 10) acting as material inside reflectors, providing readings that significantly differ from the actual values.



Figure 10 – SA 278 CL 40 micrography

Furthermore, due to the vertical casting process of such cylindrical shells, the material presents a sound velocity variation along its length, which implies that the measuring apparatus will provide thickness readings increasing along the cylinder length, from its base to its top (imagining it in vertical position during the casting process). In order to minimize this deviation, the data obtained from these readings were corrected by applying a compensation at all points along the cylindrical shell length. Fig. 11 (a) presents the thickness distribution along the longitudinal axis of the shell (each color represents one of the 28 angular positions for thickness measurements - see Fig. 9), according to the values found, Fig. 11 (b) showing the thicknesses after the above-mentioned correction.



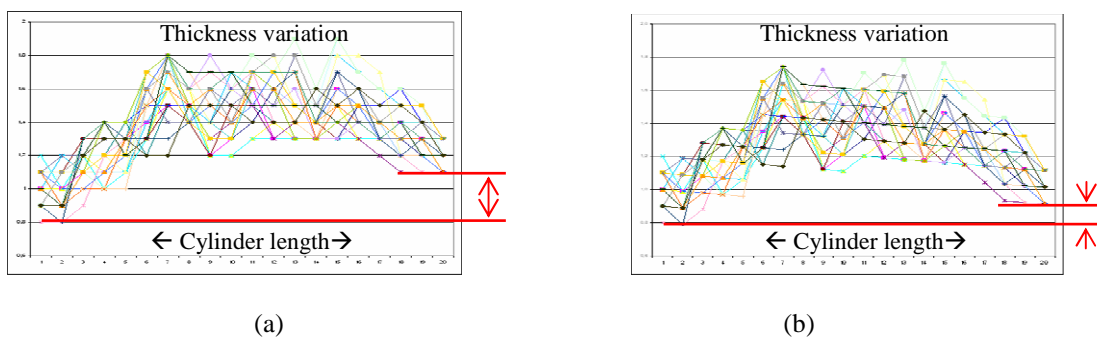(a)                                                      (b)

Figure 11 – Thickness variation along the longitudinal axis of the cylindrical shell

Thus, additional errors are supposed to be introduced into these readings, besides that already presented previously. Fig. 12 and 13 illustrate some results of the design thickness deviation mapping associated with the colors, so as to allow better visualization of its distribution:
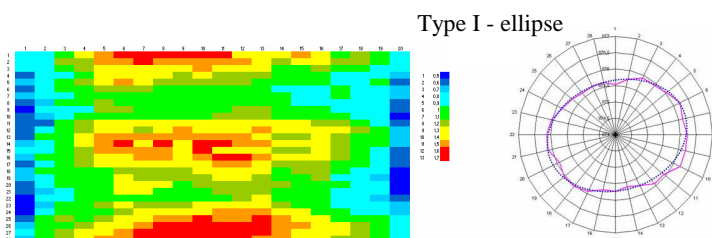


Figure 12 – Ellipse type cylindrical shell thickness variation distribution

In Fig. 12 the horizontal axis represents the cylindrical shell longitudinal direction and the vertical one its developed length (π x outside diameter). A thickness distribution can be also observed, which in this case suggests an elliptical form along most cylinder length.

Based on the measurements carried out, the shells can be grouped in the following main groups:
- **Ellipse** aspect thickness distribution (Fig. 12)
- **Eccentric circle** aspect thickness distribution (Fig. 13)
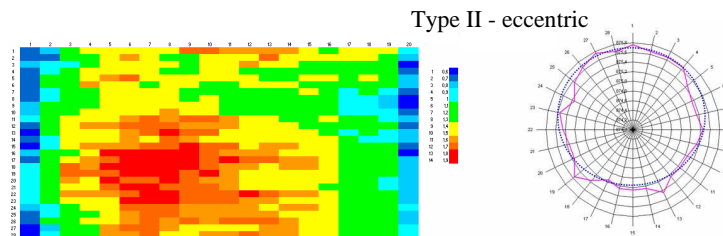
Type II - eccentric



Figure 13 – Cylindrical shell thickness variation distribution, eccentric type

## 2.2. Finite element method (FEM)

### 2.2.1. Cylindrical shell 3D modeling

Thickness measurements mentioned under 2.1.5 were used as model input data. Besides the previously described errors, some discrepancies between adjacent points indicating unreal values such as 1.6, **1.3**, 1.8. as well in longitudinal as in circumferential direction also occurred at the measurements, such values having been replaced by the result of the simple arithmetic mean of two adjacent points in one of the directions, chosen according to each case.

By using macros, the thickness measuring result were imported directly to the 3D modeling software, in which the points corresponding to the measurement were inserted for each spreadsheet column (cylindrical shell section), thus creating a spline curve (Fig. 14) through all points of that plane. After introducing all sections, a surface was generated and passed through all existing sections (loft). Later the cylindrical shell faces were longitudinally projected, so as to obtain the actual length of the cylindrical shell represented by this model.

### 2.2.2. Finite element analysis

As the 3D model was ready, the geometry was exported to finite element program ANSYS. To perform the analysis, it was decided to use high order solid elements (20 nodes) in an attempt of representing the thickness variation with reasonable precision.

In order to simulate the influence of the equipment heads, which are responsible for supporting the cylindrical shell, they were modeled by means of rigid links between the existing nodes at the ends and an element with negligible mass and inertia, located in the position corresponding to the journal centerline, thus limiting the circumferential movement of the nodes in that area, as shown in Fig. 15.
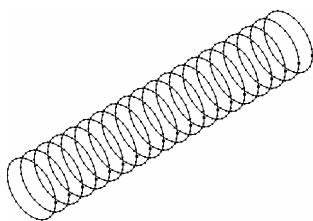


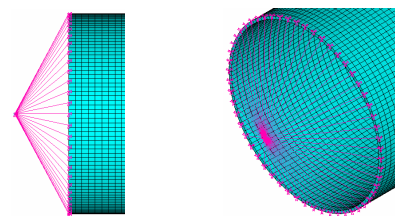Figure 14 – Sections represented by splines

Figure 15 – Representation of the rigid link between shell and bearing center

Boundary conditions were applied to the model, and at one end the movement was blocked in the three directions (using the cylindrical coordinate system), while at the other one the cylinder could move in axial direction. This boundary condition was adopted because it represents the conditions under which the cylinder had its dynamic deformation (ovalization) measured. In addition, the rotational speed of 11.72 Hz was imposed.

It is important to note that the analysis is <u>static</u> and thus it was not tried to determine any vibrations.

## 3. RESULTS AND COMMENTS

### 3.1. Simulations of cylindrical shells with imposed imperfections

Aiming to evaluate the thickness variation influence on the cylindrical shell ovalization during rotation, the following simulations were done by imposing deterministic variations.

### 3.1.1. Influence of thickness variation distribution in the central plane

It can be observed in the thickness measurements that several cylindrical shells have variations of similar magnitude among themselves, but that during rotation the ovalization amplitudes differ enormously, the cause of which is supposed to be the way in which the thickness variation distributes. Thus, some modelings were carried out by FEM with an imposed thickness variation distribution according to Eq. 1, Buelta (1997):

$$Thickness = base\ value + \Delta.sin(n.\theta) \tag{1}$$

Where:
$n=2 \rightarrow$ corresponds to an elliptical thickness variation distribution, Fig. 16 (a);
$n=3 \rightarrow$ corresponds to a distribution with three thickness variation peaks, Fig. 16 (b);
$n=4 \rightarrow$ corresponds to a distribution with four thickness variation peaks, Fig. 16 (c);
$\theta=$ angular coordinate, 0º $\rightarrow$ 360º;
$\Delta=$thickness variation, adopted=0.25 mm (initially);
*base value*= cylindrical shell average thickness, adopted=29.25 mm;



(a)                              (b)                              (c)
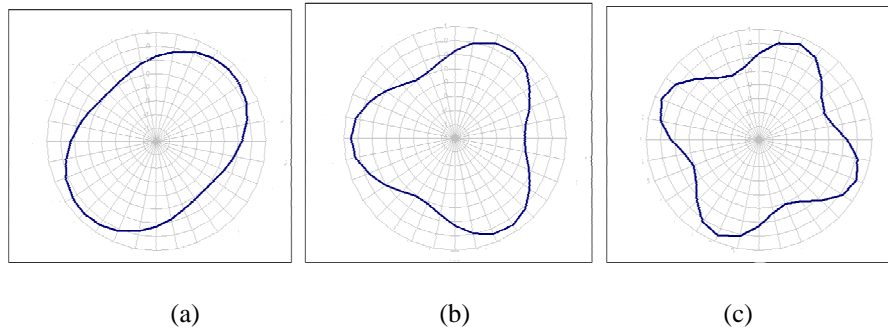Figure 16 – Thickness variation distribution

For n=2, these values generate an elliptical distribution, with 29 mm as minimum and 29.5 mm as maximum thickness.

At these models the above function was only applied to the central area, while an inside surface without variation was considered at the edges, as per Fig. 17.
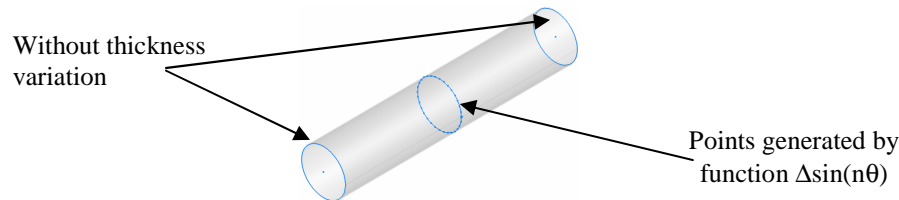


Figure 17 – Sensor measuring points according to shell rotation

The function was subdivided into 32 points and inserted in the form of a spline curve in the central plane, adopting the same procedure as mentioned under 2.2.1.

The results for 11.72 Hz are shown in Fig. 18, where it can be observed that for a same thickness variation, the more distributed it is (i.e. the higher the number of peaks), the less is the resulting cylindrical shell amplitude during rotation. Since this is a model with imposed thickness variation, the harmonics have their maximum corresponding mainly to the number of peaks that each internal geometry has i.e. at the inside distribution in the oval form the maximum is in the second harmonic (2X), at the three peak distribution the maximum is in the third harmonic and so on.
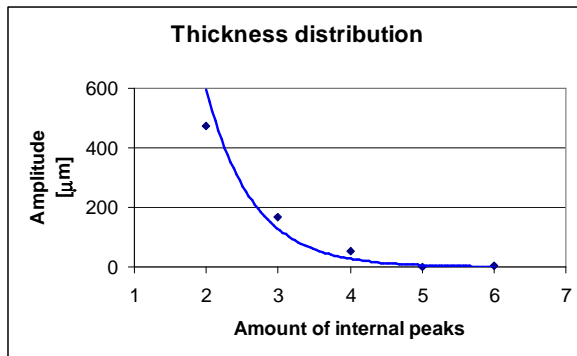
Figure 18 – Thickness distribution influence on the oval form

### 3.1.2. Influence of the number of planes with thickness variation on the ovalization

The cylinder central plane modeling was initially made, by using two central thickness measuring ranges, as shown in Fig. 19. As previously described under 2.2.1, the points describing these coordinates are inserted into a spline, considering the thickness variation at the cylindrical shell ends to be null.
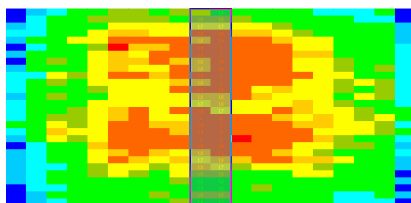


Figure 19 – Central range considered to perform a simplified model

The same operation was repeated later for four central ranges, increasing the amounts by pairs, until all cylindrical shell sections measured were encompassed.

The results obtained demonstrate that the variations are small when compared to the complete model, but the gain for making thickness measurements at future equipment shows rather expressive, since the time spent for measuring twenty planes is rather considerable, besides allowing a greater care in their accomplishment, even increasing the number of circumferential points (twenty-eight points were measured per plane). Fig. 20 illustrates the results found for cylindrical shell 16.
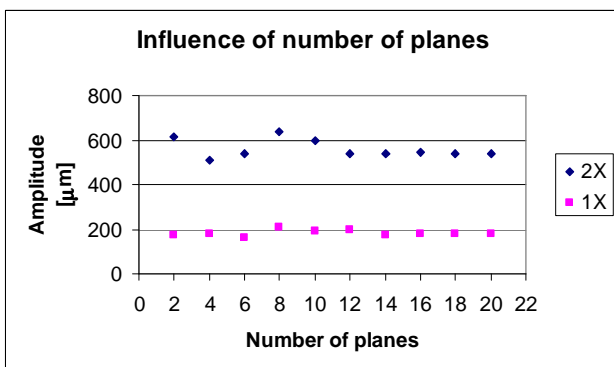


Figure 20 – Influence of the increase in the number of central planes
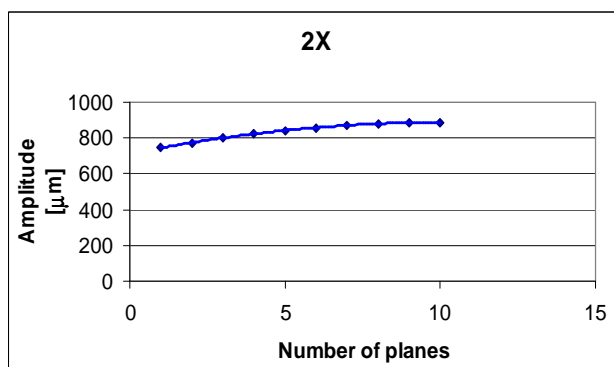


Figure 21 – Influence of the increase in the number of planes in 2X (imposed imperfection)

This occurs due to the fact that most thickness variation distribution takes place within a wide cylindrical shell central plane range.

Adopting the same procedure for an ideal theoretical cylinder with a thickness variation inside distribution in elliptical form, was obtained that shown in Fig. 21, for which the second harmonic (2X) amplitudes resulted in a quadratic distribution.

### 3.1.3. Influence of thickness variation in the central plane

In this case, making use of the elliptical form in the central plane, a fixed minimum thickness (29 mm) was adopted and the maximum thickness value was increased.

Figure 22 indicates that the amplitude of the oval form increases linearly with the thickness increase.
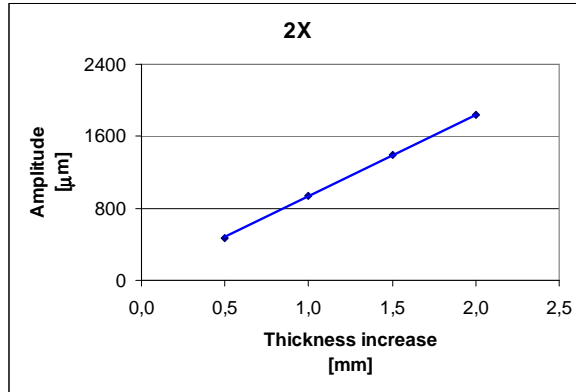


Figure 22 – Influence of thickness increase in the central plane

### 3.1.4. Influence of thickness variation in the central plane with the minimum thickness increased

The purpose of this comparison is to evaluate how much is the influence of thickness increase in the central plane on the cylindrical shell ovalization, assuming an elliptical distribution, but keeping constant the difference between maximum and minimum values - see Table 1.

Table 1 – Values used to simulate thickness variation

|  | Thickness variation | | | |
|  | I | II | III | IV |
| --- | --- | --- | --- | --- |
| Minimum | 29.0 | 29.5 | 30.5 | 31.0 |
| Maximum | 29.5 | 30.0 | 31.0 | 31.5 |
| Variation | 0.5 | 0.5 | 0.5 | 0.5 |

The results obtained are indicated in Fig. 23, in which it can be observed that an increase in thickness causes the ovalization to decrease, which should be mainly caused by an increase in the cylindrical shell rigidity in the central area.
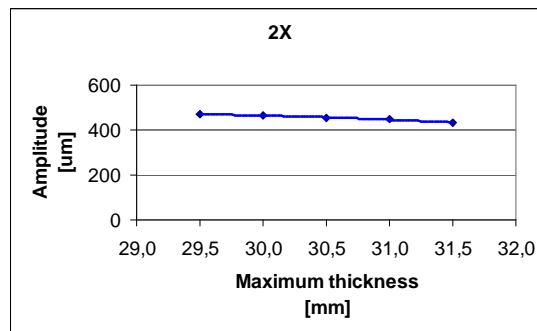


Figure 23 – Influence of minimum thickness increase

### 3.1.5. Influence of eccentric type thickness variation distribution

The inside circle center displacement was adopted at this simulation, just in the cylindrical shell central plane in 0.5 mm increments, but maintaining 29 mm as cylindrical shell minimum thickness. Figure 24 shows that the increase in eccentricity causes a linear ovalization increase. In this case the first harmonic presents the greatest participation in the cylindrical shell amplitude.
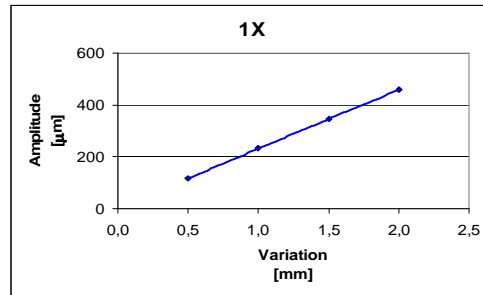
Figure 24 – Influence of eccentricity on the oval shape

### 3.1.6. Influence of speed on the cylindrical shell ovalization amplitude

Starting from a cylinder with elliptical thickness variation distribution in the central plane (minimum/maximum thicknesses = 29/29.5 mm), the rotational speed was varied to verify the cylindrical shell outside surface amplitude behavior. It is well known that this amplitude should vary with the rotational speed square. Figure 25 shows the results obtained.
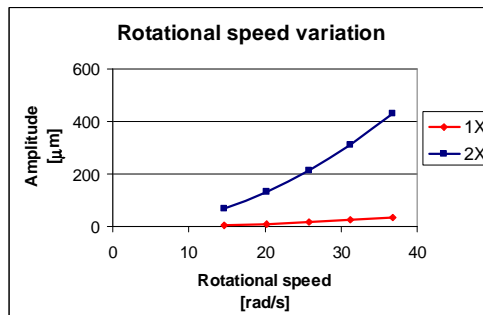


Figure 25 – Amplitude variation as a function of speed

### 3.2. Results of FEM models carried out based on thickness variation measurements

As the equipments were balanced and the shell simulations by FEM do not take account of the corrections by means of mass introduction, it does not make sense to establish comparisons between the 1X harmonics, except for thickness distribution (eccentric case). Figure 26 presents the comparison between the second harmonic (2X) of FEM model and that of the ovalization measurements carried out.
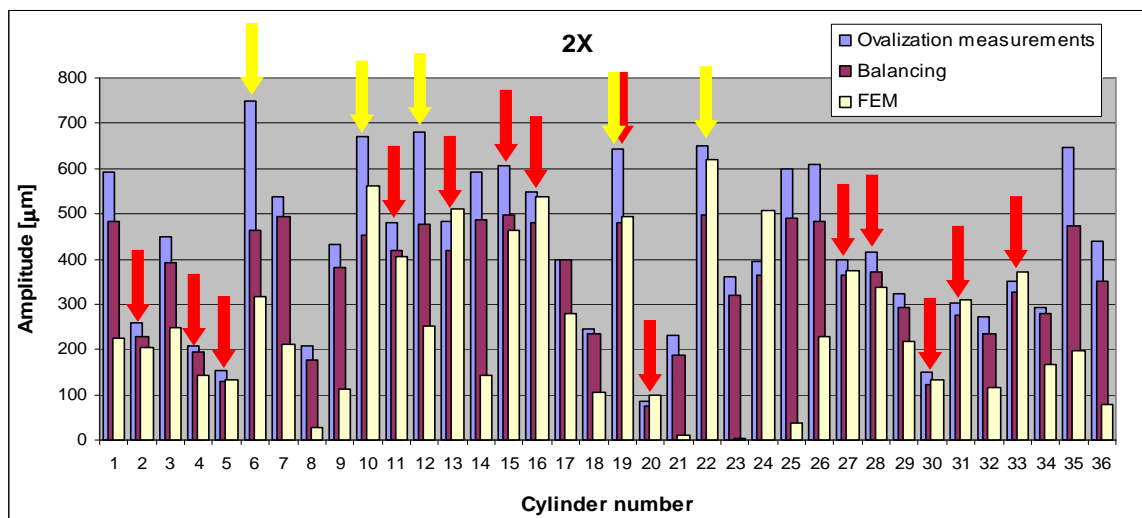


Figure 26 – Comparison between 2X results

In Fig. 26 the red arrows indicate the finite element simulation results, which are close to those of the ovalization measurements as well as by one or by both methodologies, which provides fourteen models (≈39%). It becomes evident that in most cases there is no clear relationship between them. The most probable cause for this fact are the results of thickness measurements made by ultrasound, in which, due to the fact that the graphite lamellae act as reflectors, a very high deviation from the thickness values is caused and only a measuring grid much deeper than that adopted might minimize this impact, by which procedure, on the other hand, the measuring time becomes too long and might make unviable the practical process for taking these values.

The yellow arrows indicate the cylinders described under 2.1.4, which present a discrepancy between inductive current sensor measurement results and those obtained by the balancing machine sensor measurements. At cylinders 10, 19 and 22 the finite element model approached some of 2X measurement results.

Figure 27 shows the cylindrical shell outside surface central area displacement graphs at the finite element model according to the methodology described under 2.2, where it becomes evident that the simulation is effective in reproducing the effect the shell assumes during its rotation.
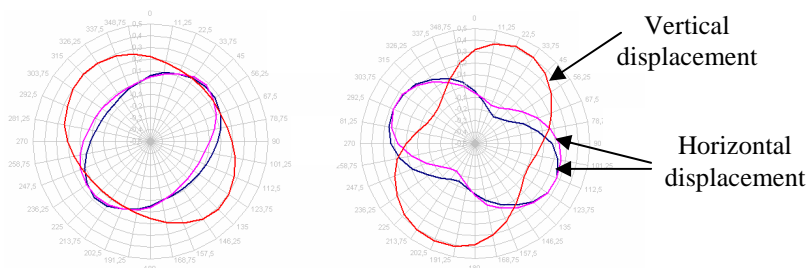


Figure 27 – Oval shape of cylinders No. 2 and 15, based on FEM

## 4. CONCLUSIONS

Apart from some exceptions, the FEM comparisons with the experimental results indicate a divergence of results in quantitative terms, the probable cause of which may be related to the errors generated in the thickness mapping, besides the correction itself of the measurements for all points in longitudinal direction, as already previously discussed.

The models with deterministically imposed thickness variation demonstrate that more important than the thickness amplitude (variation) existing inside the cylindrical shell is the way in which this variation distributes, and it may increase the cylindrical shell ovalization, while if it is altered to a more uniform inside variation distribution, an almost exponential reduction in ovalization is achieved. It can be also observed that an increase in wall thickness (even if in the central area only) causes a reduction in ovalization due to the increase in cylindrical shell rigidity. In addition, the planes located in the cylindrical shell central area are the most significant ones for ovalization formation, which will permit in future analyses to concentrate the thickness measurements in the central area, with the increase in the number of circumferential points, thus improving precision in the finite element model accomplishment.

Therefore, in a manufacturing process of this type of equipment these points are important to minimize this phenomenon.

By way of suggestion for future researches it is necessary to develop new ultrasonic thickness measuring methodologies for flake/lamellar graphite cast iron (gray cast iron) and also to verify the graphite lamella influence on the inductive current sensor results.

## 4. REFERÊNCIAS

Buelta Martinez, M. A., 1997. "A importância das imperfeições geométricas no projeto e fabricação de estruturas". São Paulo: EPUSP. Texto preparado para o concurso de professor titular no Departamento de Estruturas e Fundações da Escola Politécnica da USP.

Pires, A. C., 2006, "Desenvolvimento de ligas de ferro fundido cinzento para a fabricação de cilindros secadores utilizados em máquinas de produção de papel". 2006. 81 f. Dissertação (Mestrado) - Universidade São Francisco, Itatiba, São Paulo.

Technical Association of the Pulp and Paper Industry, 2001. TIP 0402-16: "Guidelines for inspection and nondestructive examination of paper machine dryers". US: TAPPI. 13 p.

## 5. RESPONSIBILITY NOTICE

The authors are the only responsible for the printed material included in this paper.